Structural Properties of Nuclei in the $20 \leq N\,(Z) \leq 28$ Region: Shell-Model *vs.* C.F.P. *vs.* TDHF+QNP

Kazuyuki Sekizawa[1, *]

[1] *Graduate School of Pure and Applied Sciences, University of Tsukuba, Tsukuba 305-8571, Japan*

(Submitted 10 October 2014; revised 16 December 2014)

Background: The time-dependent Hartree-Fock (TDHF) theory has been successful in describing low-energy heavy ion reactions. Recently, we have shown that multinucleon transfer (MNT) processes can be reasonably described in the TDHF theory combined with the particle-number projection technique.

Purpose: After the MNT reaction, various kinds of nuclei are produced. We theoretically investigate structural properties of those nuclei to elucidate underlying microscopic reaction mechanisms.

Methods: In this project, we investigate low-lying energy spectra of nuclei having valence nucleons in the $1f_{7/2}$ orbit on top of the $N\,(Z) = 20$ inert core. To calculate energy spectra, we use three models, the shell-model, the theory of coefficients of fractional parentage (c.f.p.), and the TDHF theory combined with a quantum-number projection (QNP) technique (TDHF+QNP). We evaluate two-body matrix elements for nuclei in the $20 \leq N\,(Z) \leq 28$ region employing an interpolation technique. For three and four particle (hole) states in a single-j orbit, we will also use a well-known theory of c.f.p. which analytically gives us expressions of energy spectra relative to the ground state. We will separately develop a theoretical framework of the TDHF theory to obtain energy spectra of reaction products specified by the total spin and parity, J^π, by extending the QNP technique.

Results: We obtain two-body particle-particle (hole-hole) and particle-hole matrix elements for all nuclei in the $20 \leq N\,(Z) \leq 28$ region by the interpolation technique. We perform shell-model calculations for those nuclei using the evaluated two-body matrix elements. Comparing energy spectra of the shell-model calculation and those of measurements, we find a fairly good agreement between them.

Perspectives: The method we have developed in this project would be useful to evaluate two-body matrix elements for many nuclei in a wide mass region. As a next step, we will develop the other approaches, the theory of c.f.p. and the TDHF+QNP, which have not been investigated yet. Combining these three approaches, we hope to develop our understands of both static and dynamical properties of atomic nuclei.

I. INTRODUCTION

Nuclear reaction experiment utilizing a large heavy-ion accelerator is indispensable to study properties of atomic nuclei. We can explore structural properties of nuclei from outcome of the reaction: various kinds of cross sections and its incident energy dependence, angular distributions, momentum distributions, energy losses, deexcitation properties of reaction products, and so on. Since reaction dynamics and nuclear structure are mutually related, to develop both nuclear structure and reaction theories is naturally requisite for developing our true understanding of atomic nuclei.

Thanks to the ongoing development of experimental apparatus, nowadays, detail studies of multinucleon transfer (MNT) processes have been becoming feasible [1]. Precise measurements of differential cross sections as well as energy and angle integrated cross sections for each transfer channel have been performed [2–5]. Moreover, decay spectroscopic studies of reaction products generated through the MNT reaction have recently been achieved by γ-particle coincidence technique [6].

To understand the microscopic reaction mechanisms of the MNT reaction, we have studied MNT processes employing the time-dependent Hartree-Fock (TDHF) theory [7–10]. As a first attempt, we studied MNT processes in low-energy heavy ion reactions at around the Coulomb barrier for several systems for which measured cross sections have been available [7]. From the thorough analysis reported in Ref. [7], we have concluded that MNT cross sections can be quantitatively described by the microscopic TDHF theory combined with the particle-number projection (PNP) technique [11].

Recently, we have developed a theoretical framework to calculate expectation values of operators in the TDHF wave function after collision with the PNP [9]. This method enables us to investigate properties of reaction products generated though the MNT reaction within the microscopic framework of the TDHF theory. However, because we have included only the PNP in our theoretical framework, obtainable expectation values are averaged over all possible quantum states populated by the reaction. To get deeper insight into reaction mechanisms as well as structure of reaction products, it is desirable to extend our framework to include party and angular momentum projections [12]. It is then possible to analyze excited states of reaction products specified by the

* sekizawa@nucl.ph.tsukuba.ac.jp

total spin and parity, J^π. We shall refer this approach, the TDHF theory combined with the quantum-number projection (QNP) technique, as "TDHF+QNP" in this project.

Based on the above, the aim of this project has become to develop theoretical models which can be applied to a number of nuclei in the wide mass region, to investigate properties of reaction products generated through MNT processes. In this project, we are planing to use three models, (*i*) the shell-model, (*ii*) the theory of coefficients of fractional parentage (c.f.p.) [19], and (*iii*) the TDHF+QNP. Specific meaning to use them are the followings:

(*i*)**:** As is well-known, the nuclear shell-model has been successful to describe various properties of atomic nuclei (e.g. magic numbers, single-particle energies, ground state spin-parity, low-lying excitation spectra, and so on). Thus, energy spectra evaluated by using the shell-model would be a good reference results to examine whether the shell-model picture, which assumes independent particles in a one-body mean-field potential, and its assumption on the model-space are valid or not. Therefore, in this project, we develop a method to evaluate two-body matrix elements, which are necessary for the shell-model calculation, to calculate energy spectra of many nuclei.

(*ii*)**:** When we consider low-lying states of a nucleus which has a core plus valence nucleons in a single-j orbit, the theory of c.f.p. provides a elegant prescription to describe excited states as a simple coupling scheme of the valence nucleons [19]. It would be an indicator that tells us whether those excited states can be constructed from the simple coupling scheme or not. We will thus compare energy spectra evaluated by other methods with the predictions of c.f.p.

Actually, in the above two approaches, we consider just a *static* structural properties. We then need the third approach to examine *dynamical* aspects and reaction mechanisms:

(*iii*)**:** Apart from (*i*) and (*ii*), we calculate heavy ion reactions using the TDHF theory to obtain the many-body wave function after collision. Achieving an extension of our formalism to include the parity and angular momentum projections, we would get energy spectra from the TDHF wave function after collision. The energy spectra obtained from the TDHF+QNP may include not only structural properties of reaction products at a certain time $t = t_f$ after the collision but also dynamical properties of the reaction process.

From comparisons between these three approaches, we may get information of structural properties of reaction products whether it can be explained by the naive shell-model and/or c.f.p.'s considerations. This is the main interest which urged me to do this project.

This project report is organized as follows. In Sec. II, we present gross properties of nuclei in the target region, $20 \leq N\,(Z) \leq 28$, which are useful to proceed our consideration. In Sec. III, we explain our methods to evaluate structural properties of those objective nuclei. In Sec. IV, a summary and a perspective are presented.

II. GROSS STRUCTURAL PROPERTIES

For simplicity, in this project, we concentrate on nuclei with valence nucleons in the $1f_{7/2}$ orbit. We assume that N and $Z = 20$ cores are inert. Before explaining our approaches to investigate low-lying energy spectra of those nuclei, we show gross properties of objective nuclei which would be useful to proceed our consideration.

A. Half-life

In Fig. 1, we show a part of nuclear chart which shows all nuclei in the objective region, $20 \leq N\,(Z) \leq 28$. Each box corresponds to each nucleus. The box color represents the half-life, $T_{1/2}$, of corresponding nucleus. Stable nuclei with $T_{1/2} > 10^{15}$ s are represented by black boxes. Blue, cyan, and dark-green boxes represent nuclei with half-lives $T_{1/2} \sim 10^{10}$ s, 10^{5-7} s, and 10^4 s, respectively. Light-green boxes located in $N \leq Z$ region represent nuclei with half-lives $T_{1/2} \lesssim 10^{-1}$ s. As seen from the figure, proton-rich nuclei in this region have rather short half-lives. We indeed find that energy spectra of those proton-rich nuclei are still not well-known. We will thus compare

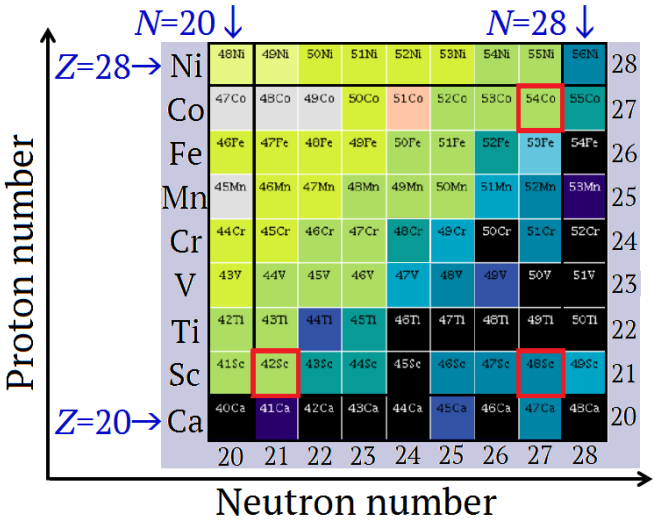

FIG. 1. (Color online) A part of nuclear chart which shows objective nuclei in this project. Box color indicates the half-life of each nucleus (for more detail see text). The chart has been taken from Ref. [13]. Red square boxes indicate key nuclei whose two-body matrix elements are determined from available experimental data. These matrix elements are used in the interpolation procedure (see text).

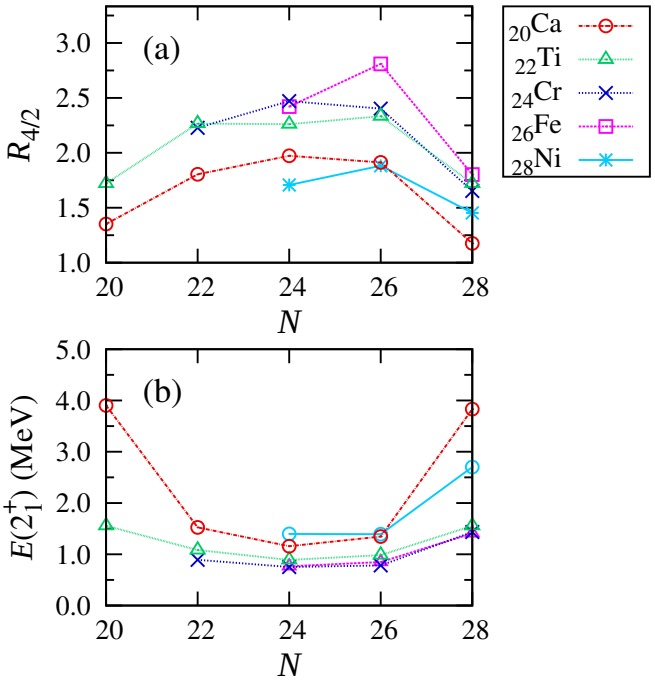

FIG. 2. (Color online) $R_{4/2}$ ratio (a) and excitation energy of first 2^+ state (b) are shown for even-even nuclei in the $20 \leq N\,(Z) \leq 28$ region as functions of the neutron number.

calculated energy spectra with those of measurements for nuclei in $N \geq Z$ region.

B. $R_{4/2}$ and $E(2_1^+)$

It is well-known that the ratio of excitation energy of first 4^+ state to that of first 2^+ state, $R_{4/2} \equiv E(4_1^+)/E(2_1^+)$, would be a measure of collectivity and shape evolution. Nuclei having vibrational nature, which exhibit quadrupole-phonon excitation modes at low excitation energy, give $R_{4/2} \sim 2$. While nuclei having rotational nature (well deformed nuclei which has a sharp minimum of the potential energy surface on the β-γ plane showing $J(J+1)$ rotational band) give $R_{4/2} \sim 3.33$. Let us take a look at experimental data of the $R_{4/2}$ ratio and the value of $E(2_1^+)$ for even-even nuclei reported in Ref. [13].

In Fig. 2, we show the $R_{4/2}$ ratio in panel (a) and the value of $E(2_1^+)$ in panel (b) as functions of the neutron number, N. Red open circles, green open triangles, blue crosses, pink squares, and cyan stars connected with lines show results of $_{20}$Ca-, $_{22}$Ti-, $_{24}$Cr-, $_{26}$Fe-, and $_{28}$Ni-isotopes, respectively.

From the figure, we find that rather small values of $R_{4/2}$ ratio for all nuclei except for $^{52}_{26}\mathrm{Fe}_{26}$ which has $R_{4/2} \sim 2.8$ (but still lower than 2.9, a critical value for shape transition). Especially, for nuclei with the magic number $N = 20, 28$ and/or $Z = 20, 28$, we find that the $R_{4/2}$ ratio takes values smaller than two, indicating a substantial shell effect which suppresses excitations of quadrupole phonons. From these values, we expect a small deformation for nuclei in this region and a good description by spherical shell-model calculations for them. We note that the ground-state spin-parity of nuclei having $N = 21, 23, 25, 27$ and $Z = 20$ and having $Z = 21, 23, 25, 27$ and $N = 20$ are always $J^\pi = 7/2^-$. This fact would also suggest a persistence of spherical shell-model picture for those nuclei.

C. Energies of low-lying excited states

From the above consideration, we find possible indications that we may reasonably assume the spherical shell-model configuration for nuclei in the $20 \leq N\,(Z) \leq 28$ region. We thus apply the m-scheme to investigate low-lying energy spectra of nuclei having 2-particle (2p), 2-hole (2h), and 1-particle 1-hole (1p1h) configurations, in the $1f_{7/2}$ orbit. For two identical particles (holes), the m-scheme predicts states with total angular momentum $\lambda = 0, 2, 4$, and 6. For a neutron and a proton particles (holes), the m-scheme predicts states with total angular momentum $\lambda = 0, 1, \cdots, 7$, because of the lack of the Pauli exclusion principle.

In Table I, we show measured low-lying excitation energies specified by $J^\pi = 0^+, 1^+, \cdots, 7^+$ for nuclei with 2p, 2h, and 1p1h configurations. As we expected from the m-scheme, we indeed find those states at low excitation energies in experimental spectra. Since $^{50}_{28}\mathrm{Ni}_{22}$, $^{46}_{26}\mathrm{Ni}_{20}$, and $^{48}_{27}\mathrm{Ni}_{21}$, are extremely proton-rich and they are almost on the proton drip-line, energy spectra of those nuclei have not been measured experimentally. Such unknown states are represented by hyphens, "−", in Table I.

For $^{42}_{21}\mathrm{Sc}_{21}$ and $^{54}_{27}\mathrm{Co}_{27}$ nuclei, there are several states whose spin-parity, J^π, has not been identified experimentally. If there are several candidate states for a single spin-parity, we have arbitrary selected one state from among those candidates. Their energies are represented with parenthesis in the table. We have selected the 5^+ state of $^{42}_{21}\mathrm{Sc}_{21}$ as a state at $E^* \sim 1.5$ MeV, because it has a similar energy to the energy of the 5^+ state in $^{54}_{27}\mathrm{Co}_{27}$. Similarly, we have selected the 6^+ states of $^{42}_{21}\mathrm{Sc}_{21}$ and $^{54}_{27}\mathrm{Co}_{27}$ as states at $E^* \sim 3.2$ MeV and $E^* \sim 2.9$ MeV, because 6^+ states of all nuclei with 2p or 2h configuration emerge at around 3 MeV (see columns 2-5, 7, and 9). The 7^+ state of $^{42}_{21}\mathrm{Sc}_{21}$ is selected because it is the candidate with lowest energy and other candidates have much higher energy, more than 3 MeV.

From the table, we find that excitation energies of 2^+, 4^+, and 6^+ states are very similar to each other independent from whether two states are particle-states or hole-states and from their isospins. It may indicate an existence of particle-hole symmetry as well as isospin symmetry in residual interactions acting on valence nucleons in the $1f_{7/2}$ orbit. In the next Section, we will use this fact to evaluate two-body matrix elements for all nuclei in the $20 \leq N\,(Z) \leq 28$ region by an interpolation technique.

TABLE I. Measured low-lying excitation energies for nuclei with core+two-particle (2p), core+two-hole (2h), or core+one-particle-one-hole (1p1h) configurations in the $20 \le N\,(Z) \le 28$ region are shown. Experimental data have been taken from Ref. [13]. Energies with parenthesis mean that its spin-parity J^π has not been identified yet (see text for more detail). States which have not been measured are represented by hyphens, "–".

	$E^*_{\rm exp}(N,Z;J^\pi)$ (MeV)											
	$^{42}_{20}$Ca$_{22}$	$^{46}_{20}$Ca$_{26}$	$^{42}_{22}$Ti$_{20}$	$^{50}_{22}$Ti$_{28}$	$^{50}_{28}$Ni$_{22}$	$^{54}_{28}$Ni$_{26}$	$^{46}_{26}$Fe$_{20}$	$^{54}_{26}$Fe$_{28}$	$^{42}_{21}$Sc$_{21}$	$^{54}_{27}$Co$_{27}$	$^{48}_{21}$Sc$_{27}$	$^{48}_{27}$Co$_{21}$
J^π	(2p$^\nu$)	(2h$^\nu$)	(2p$^\pi$)	(2p$^\pi$)	(2p$^\nu$)	(2h$^\nu$)	(2h$^\pi$)	(2h$^\pi$)	(1p$^\pi$1p$^\nu$)	(1h$^\pi$1h$^\nu$)	(1p$^\pi$1h$^\nu$)	(1h$^\pi$1p$^\nu$)
7^+									(0.616)	0.197	1.096	–
6^+	3.189	2.974	3.043	3.199	–	3.071	–	2.949	(3.242)	(2.912)	0.000	–
5^+									(1.510)	1.887	0.131	–
4^+	2.752	2.575	2.677	2.675	–	2.620	–	2.538	2.815	2.652	0.252	–
3^+									1.490	1.822	0.623	–
2^+	1.525	1.346	1.556	1.554	–	1.392	–	1.408	1.586	1.446	1.143	–
1^+									0.611	0.937	2.517†	–
0^+	0.000	0.000	0.000	0.000	0.000	0.000	0.000	0.000	0.000	0.000	6.678	–

†Although there has also been measured a $J^\pi = 1^+$ state at $E^* \sim 2.2$ MeV, we have taken the $J^\pi = 1^+$ state at $E^* \sim 2.5$ MeV as a member of particle-hole multiplet, because the latter is much more populated than the former in various reactions, *e.g.* ^{48}Ca(p,n), ^{48}Ca$(^3$He$,t)$, and ^{48}Ti$(t,^3$He$)$ reactions [14].

III. METHODS AND RESULTS

A. Evaluation of two-body matrix elements

We define a shell-model interaction for the $1f_{7/2}$ orbit which can be applied to nuclei in the $20 \le N\,(Z) \le 28$ region. We first determine two-body interaction matrix elements for $^{42}_{21}$Sc$_{21}$, $^{54}_{27}$Co$_{27}$, and $^{48}_{21}$Sc$_{27}$ from available experimental spectra. We will then construct two-body matrix elements for other nuclei employing an interpolation technique.

1. Determination from experimental spectra

We can directly determine particle-particle, hole-hole, and particle-hole matrix elements, $v^{\rm pp}_\lambda$, $v^{\rm hh}_\lambda$, and $v^{\rm ph}_\lambda$, respectively, using available experimental data of low-lying energy spectra shown in Table I and nuclear binding energies of neighboring nuclei, as follows.

As shown in Table I, we found low-lying states which can be considered as a particle-particle (hole-hole, or particle-hole) multiplet in the experimental spectra. Because of our assumption that there exist $N = 20$ or 28 and/or $Z = 20$ or 28 inert core, we can regard excitation energies of those states as relative values of two-body matrix elements of the residual interaction for the valence nucleons.

The absolute value of the matrix elements for the ground state can be determined from the binding energies of the neighboring nuclei. Let us first consider the case of particle-particle matrix elements. By taking a difference between nuclear binding energies, we may obtain a relation, $B\left[^{42}_{21}\mathrm{Sc}_{21}\right] - B\left[^{40}_{20}\mathrm{Ca}_{20}\right] \approx -v^{\rm pp}_0 - V^{\rm p}_\nu - V^{\rm p}_\pi$, where B denotes the nuclear binding energy of the specified nucleus in the square brackets. The $-V^{\rm p}_\tau$ denotes an interaction energy between a particle-state with isospin τ and the other nucleons. In the same way, we may obtain $B\left[^{41}_{21}\mathrm{Sc}_{20}\right] - B\left[^{40}_{20}\mathrm{Ca}_{20}\right] \approx -V^{\rm p}_\pi$ and $B\left[^{41}_{20}\mathrm{Ca}_{21}\right] - B\left[^{40}_{20}\mathrm{Ca}_{20}\right] \approx -V^{\rm p}_\nu$. By combining these three relations, we may determine the absolute value of the ground state matrix element $v^{\rm pp}_0$ by

$$\begin{aligned} v^{\rm pp}_0 &= -B\left[^{40}_{20}\mathrm{Ca}_{20}\right] - B\left[^{42}_{21}\mathrm{Sc}_{21}\right] + B\left[^{41}_{21}\mathrm{Sc}_{20}\right] + B\left[^{41}_{20}\mathrm{Ca}_{21}\right] \\ &= -342.034 - 354.667 + 343.117 + 350.397 \\ &= -3.187 \quad \text{(MeV)}. \end{aligned} \tag{1}$$

We have evaluated the nuclear binding energy from atomic binding energies reported in AME2003, the atomic mass evaluation [16], correcting the electrons' binding energy according to Eqs. (A2) and (A4) in Ref. [17]. After the determination of the absolute value of $v^{\rm pp}_0$, we evaluate other matrix elements relative to the $v^{\rm pp}_0$ by $v^{\rm pp}_{\lambda\neq 0} = v^{\rm pp}_0 + E^*_{\rm exp}(\lambda)$. The resulting particle-particle matrix elements for the $1f_{7/2}$ orbit deduced from the experimental energy spectrum of $^{42}_{21}$Sc$_{21}$ are shown in column 2 of Table II.

In a similar manner, we determine absolute values of

TABLE II. Particle-particle matrix elements $v_\lambda^{\rm pp}$ in the $1f_{7/2}$ orbit deduced from the energy spectrum of $^{42}_{21}\mathrm{Sc}_{21}$. Particle-hole interaction matrix elements $v_\lambda^{\rm ph}$, which are evaluated from the $v_\lambda^{\rm pp}$ through the Pandya transformation Eq. (4), are also shown.

Sc42			
(λ, T)	$v_\lambda^{\rm pp}$ (MeV)	(λ, T)	$v_\lambda^{\rm ph}$ (MeV)
$(6, 1)$	0.055	$(0, 1)$	-13.835
$(4, 1)$	-0.372	$(1, 0)$	-18.478
$(2, 1)$	-1.601	$(7, 0)$	-19.685
$(5, 0)$	-1.677	$(3, 0)$	-20.475
$(3, 0)$	-1.697	$(2, 1)$	-20.546
$(7, 0)$	-2.571	$(4, 1)$	-20.753
$(1, 0)$	-2.576	$(5, 0)$	-20.785
$(0, 1)$	-3.187	$(6, 1)$	-20.873

hole-hole and particle-hole matrix elements by

$$\begin{aligned} v_0^{\rm hh} &= -B\left[^{56}_{28}\mathrm{Ni}_{28}\right] - B\left[^{54}_{27}\mathrm{Co}_{27}\right] + B\left[^{55}_{27}\mathrm{Co}_{28}\right] + B\left[^{55}_{28}\mathrm{Ni}_{27}\right] \\ &= -483.951 - 462.700 + 476.789 + 467.311 \\ &= -2.550 \quad (\mathrm{MeV}), \end{aligned} \tag{2}$$

$$\begin{aligned} v_6^{\rm ph} &= -B\left[^{48}_{20}\mathrm{Ca}_{28}\right] - B\left[^{48}_{21}\mathrm{Sc}_{27}\right] + B\left[^{49}_{21}\mathrm{Sc}_{28}\right] + B\left[^{47}_{20}\mathrm{Ca}_{27}\right] \\ &= -415.972 - 415.469 + 425.597 + 406.027 \\ &= 0.182 \quad (\mathrm{MeV}). \end{aligned} \tag{3}$$

We note that total angular momentum λ of the ground state of $^{48}_{21}\mathrm{Sc}_{27}$ is six as shown in column 12 of Table I. The resulting hole-hole and particle-hole matrix elements are shown in column 2 of Table III and IV, respectively.

TABLE III. Same as Table I but for hole-hole matrix elements $v_\lambda^{\rm hh}$ deduced from the energy spectrum of $^{54}_{27}\mathrm{Co}_{27}$. Particle-hole matrix elements $v_\lambda^{\rm ph}$, which are evaluated from the $v_\lambda^{\rm hh}$ through the Pandya transformation Eq. (4), are also shown.

Co54			
(λ, T)	$v_\lambda^{\rm hh}$ (MeV)	(λ, T)	$v_\lambda^{\rm ph}$ (MeV)
$(6, 1)$	0.594	$(0, 1)$	-2.456
$(4, 1)$	0.381	$(1, 0)$	-5.257
$(5, 1)$	-0.663	$(7, 1)$	-7.464
$(3, 0)$	-0.728	$(2, 0)$	-7.490
$(2, 0)$	-1.104	$(3, 1)$	-7.811
$(1, 0)$	-1.613	$(4, 0)$	-8.327
$(7, 0)$	-2.353	$(5, 1)$	-8.517
$(0, 1)$	-2.550	$(6, 0)$	-8.609

TABLE IV. Same as Table II and III but for particle-hole matrix elements $v_\lambda^{\rm ph}$ deduced from the energy spectrum of $^{48}_{21}\mathrm{Sc}_{27}$. Particle-particle matrix elements $v_\lambda^{\rm pp}$, which are evaluated from the $v_\lambda^{\rm ph}$ through the inverted Pandya transformation Eq. (6), are also shown.

Sc48			
(λ, T)	$v_\lambda^{\rm ph}$ (MeV)	(λ, T)	$v_\lambda^{\rm pp}$ (MeV)
$(0, 3)$	6.860	$(6, 1)$	0.594
$(1, 3)$	2.699	$(4, 1)$	0.381
$(2, 3)$	1.325	$(2, 1)$	-0.496
$(7, 3)$	1.278	$(5, 0)$	-0.549
$(3, 3)$	0.805	$(3, 0)$	-0.729
$(4, 3)$	0.434	$(1, 0)$	-1.800
$(5, 3)$	0.313	$(0, 1)$	-1.807
$(6, 4)$	0.182	$(7, 0)$	-1.956

2. *Pandya transformation*

Up to now, we have determined particle-particle matrix elements $v_\lambda^{\rm pp}$ for $^{42}_{21}\mathrm{Sc}_{21}$, hole-hole matrix elements $v_\lambda^{\rm hh}$ for $^{54}_{27}\mathrm{Co}_{27}$, and particle-hole matrix elements $v_\lambda^{\rm ph}$ for $^{48}_{21}\mathrm{Sc}_{27}$, from available experimental data. There is a useful transformation which enables us to connect $v_\lambda^{\rm ph}$ and $v_\lambda^{\rm pp}$ (or $v_\lambda^{\rm hh}$) (and vice versa), the Pandya transformation [18].

The Pandya transformation is given by

$$v_\lambda^{\rm ph} = E_0 - \sum_{\lambda'} (2\lambda' + 1) \begin{Bmatrix} j & j & \lambda \\ j & j & \lambda' \end{Bmatrix} v_{\lambda'}^{\rm pp}, \tag{4}$$

where the curly brackets in Eq. (4) represent the Wigner's $6j$-symbol [19]. E_0 denotes a λ-independent interaction energy,

$$E_0 = \frac{1}{2j+1} \sum_{\text{all } \lambda'} (2\lambda'+1) v_{\lambda'}^{\rm pp} + \frac{2j-1}{2j+1} \sum_{\text{even } \lambda'} (2\lambda'+1) v_{\lambda'}^{\rm pp}, \tag{5}$$

which takes a value of $E_0 = -21.685$ MeV for $v_\lambda^{\rm pp}$ deduced from ^{42}Sc and $E_0 = -8.716$ MeV for $v_\lambda^{\rm hh}$ deduced from ^{54}Co. In column 4 of Table I and II, we show particle-hole matrix elements evaluated from $v_\lambda^{\rm pp}$ and $v_\lambda^{\rm hh}$ through the Pandya transformation Eq.(4), respectively.

We can derive an inverted version of the Pandya transformation [15]. The inverted Pandya transformation is given by

$$v_\lambda^{\rm pp} = E_0 - \sum_{\lambda'} (2\lambda' + 1) \begin{Bmatrix} j & j & \lambda \\ j & j & \lambda' \end{Bmatrix} v_{\lambda'}^{\rm ph}, \tag{6}$$

where E_0 denotes the same λ-independent interaction energy as Eq.(5) but now which is expressed by means of particle-hole matrix elements $v_\lambda^{\rm ph}$,

$$E_0 = \frac{1}{2j(2j+1)} \sum_{\lambda'} (2\lambda'+1) v_{\lambda'}^{\rm ph} - \frac{2j-1}{2j(2j+1)} v_0^{\rm ph}. \tag{7}$$

For $v_\lambda^{\rm ph}$ deduced from the experimental spectrum of ${}^{48}_{21}\mathrm{Sc}_{27}$, it is found to be $E_0 = 0.267$ MeV. In column 4 of Table IV, we show particle-particle matrix elements evaluated from $v_\lambda^{\rm ph}$ through the inverted Pandya transformation Eq. (6).

3. Interpolation technique

As we saw in Table I, the particle-particle matrix elements (columns 2, 4, and 5) have very similar values to those of the hole-hole matrix elements (columns 3 and 7) and they are not so much dependent on the isospin degrees of freedom. This fact may indicate presence of the particle-hole symmetry as well as the isospin symmetry in the two-body matrix elements between particle(s) and/or hole(s) in the $1f_{7/2}$ orbit.

Assuming the particle-hole symmetry, we obtain hole-particle matrix elements, $v_\lambda^{\rm hp}$, for ${}^{48}_{27}\mathrm{Co}_{21}$, from the evaluated $v_\lambda^{\rm ph}$ for ${}^{48}_{21}\mathrm{Sc}_{27}$. We also obtain particle-particle matrix elements, $v_\lambda^{\rm pp}$, for ${}^{54}_{27}\mathrm{Co}_{27}$, from the evaluated $v_\lambda^{\rm hh}$ for ${}^{54}_{27}\mathrm{Co}_{27}$. These four matrix elements are located at the four corners of the square region $21 \le N\,(Z) \le 27$. It means that if we interpolate the matrix elements between these four, we may obtain all two-body matrix elements available for the $21 \le N\,(Z) \le 27$ region.

We thus interpolate these matrix elements employing a simple linear interpolation technique. Here, for convenience, let us introduce a notation for two-body matrix elements, $v_\lambda^{\rm pp}(N,Z)$ and $v_\lambda^{\rm ph}(N,Z)$, where (N,Z) denotes a set of neutron and proton numbers to which these matrix elements can be applied. We first interpolate two matrix elements between $v_\lambda^{\rm pp}(21,21)$ and $v_\lambda^{\rm pp}(27,21)$ by

$$v_\lambda^{\rm pp}(N,21) = v_\lambda^{\rm pp}(21,21) + \big(N-21\big)\,\frac{v_\lambda^{\rm pp}(27,21) - v_\lambda^{\rm pp}(21,21)}{6}, \quad (8)$$

which provides particle-particle matrix elements for ${}^{43-47}\mathrm{Sc}$. In the same way, we interpolate particle-particle matrix elements $v_\lambda^{\rm pp}(27,21)$ and $v_\lambda^{\rm pp}(27,27)$ by

$$v_\lambda^{\rm pp}(27,Z) = v_\lambda^{\rm pp}(27,21) + \big(Z-21\big)\,\frac{v_\lambda^{\rm pp}(27,27) - v_\lambda^{\rm pp}(27,21)}{6}, \quad (9)$$

which provides particle-particle matrix elements for $N = 27$ isotones having proton number $22 \le Z \le 26$. We also interpolate between $v_\lambda^{\rm pp}(21,21)$ and $v_\lambda^{\rm pp}(27,27)$ by

$$v_\lambda^{\rm pp}(N,Z=N) = v_\lambda^{\rm pp}(21,21) + \big(N-21\big)\,\frac{v_\lambda^{\rm pp}(27,27) - v_\lambda^{\rm pp}(21,21)}{6}, \quad (10)$$

which provides particle-particle matrix elements for $N = Z$ nuclei. Finally, we achieve interpolations for isotones with $22 \le N \le 26$ using matrix elements evaluated by Eqs. (8) and (10) as

$$v_\lambda^{\rm pp}(N,Z) = v_\lambda^{\rm pp}(N,21) + \big(Z-21\big)\,\frac{v_\lambda^{\rm pp}(N,Z=N) - v_\lambda^{\rm pp}(N,21)}{N-21}. \quad (11)$$

These interpolations Eqs. (8-11) enables us to fill the lower triangle region, $Z \le N$ part of the $21 \le N\,(Z) \le 27$ region. Because of the particle-hole symmetry, they are equivalent to the matrix elements in the upper triangle region, $Z \ge N$ part of the $21 \le N\,(Z) \le 27$ region. To evaluate two-body matrix elements for $Z = 21$ and 28 isotopes and $N = 20$ and 28 isotones, we separately achieve similar interpolations of the matrix elements for $Z = 20$, 28 isotopes and $N = 20$, 28 isotones.

In this way, we have constructed two-body matrix elements, $v_\lambda^{\rm pp}(= v_\lambda^{\rm hh})$ and $v_\lambda^{\rm ph}(= v_\lambda^{\rm hp})$, for all nuclei in the $20 \le N\,(Z) \le 28$ region except for 12 nuclei with 0p0h, 1p0h, and 0p1h configurations.

B. Shell-model calculations

Using the two-body matrix elements evaluated in the previous Subsection, we perform shell-model calculations using the `ArbModel` [20].

1. Hamiltonian

Before showing results of the shell-model calculations, we present some details of the calculations. We denote the creation and annihilation operators for a proton particle-state (or a neutron particle-state) in the $1f_{7/2}$ orbit as $\hat{a}_\tau^{\rm p\dagger}$ and $\hat{a}_\tau^{\rm p}$, respectively, where $\tau = \pi$ for protons and $\tau = \nu$ for neutrons. Those for hole-states are denoted as $\hat{a}_\tau^{\rm h\dagger}$ and $\hat{a}_\tau^{\rm h}$. We use a standard notation of tensor couplings: a coupling of two operators $\hat{A}$ and $\hat{B}$ to a tensor having angular momentum J with its projection M_J is expressed as $\big[\hat{A}\times\hat{B}\big]^{(J)}_{M_J}$.

The Hamiltonian of the system is given as a sum of several parts:

(i) Interactions between proton particle-states,

$$\sum_{ijkl}\sum_{\lambda} v_\lambda^{\rm pp}(N,Z)\Big[\big[\hat{a}_{i,\pi}^{\rm p\dagger}\times\hat{a}_{j,\pi}^{\rm p\dagger}\big]^{(\lambda)}\times\big[\hat{a}_{k,\pi}^{\rm p}\times\hat{a}_{l,\pi}^{\rm p}\big]^{(\lambda)}\Big]^{(0)}_0,$$

or interactions between proton hole-states,

$$\sum_{ijkl}\sum_{\lambda} v_\lambda^{\rm hh}(N,Z)\Big[\big[\hat{a}_{i,\pi}^{\rm h\dagger}\times\hat{a}_{j,\pi}^{\rm h\dagger}\big]^{(\lambda)}\times\big[\hat{a}_{k,\pi}^{\rm h}\times\hat{a}_{l,\pi}^{\rm h}\big]^{(\lambda)}\Big]^{(0)}_0,$$

which are switched on when the number of proton particle-states (or hole-states) is greater than one.

(ii) Interactions between neutron particle-states,

$$\sum_{ijkl}\sum_{\lambda} v_\lambda^{\rm pp}(N,Z)\Big[\big[\hat{a}_{i,\nu}^{\rm p\dagger}\times\hat{a}_{j,\nu}^{\rm p\dagger}\big]^{(\lambda)}\times\big[\hat{a}_{k,\nu}^{\rm p}\times\hat{a}_{l,\nu}^{\rm p}\big]^{(\lambda)}\Big]^{(0)}_0,$$

or interactions between neutron hole-states,

$$\sum_{ijkl}\sum_{\lambda} v_\lambda^{\rm hh}(N,Z)\Big[\big[\hat{a}_{i,\nu}^{\rm h\dagger}\times\hat{a}_{j,\nu}^{\rm h\dagger}\big]^{(\lambda)}\times\big[\hat{a}_{k,\nu}^{\rm h}\times\hat{a}_{l,\nu}^{\rm h}\big]^{(\lambda)}\Big]^{(0)}_0,$$

which are switched on when the number of neutron particle-states (or hole-states) is greater than one.

(*iii*) Interactions between proton particle-states and neutron particle-states,

$$\sum_{ijkl}\sum_{\lambda} v_{\lambda}^{\rm pp}(N,Z)\Big[\big[\hat{a}_{i,\pi}^{\rm p\dagger}\times\hat{a}_{j,\nu}^{\rm p\dagger}\big]^{(\lambda)}\times\big[\hat{a}_{k,\pi}^{\rm p}\times\hat{a}_{l,\nu}^{\rm p}\big]^{(\lambda)}\Big]_{0}^{(0)},$$

or interactions between proton hole-states and neutron hole-states,

$$\sum_{ijkl}\sum_{\lambda} v_{\lambda}^{\rm hh}(N,Z)\Big[\big[\hat{a}_{i,\pi}^{\rm h\dagger}\times\hat{a}_{j,\nu}^{\rm h\dagger}\big]^{(\lambda)}\times\big[\hat{a}_{k,\pi}^{\rm h}\times\hat{a}_{l,\nu}^{\rm h}\big]^{(\lambda)}\Big]_{0}^{(0)},$$

which are switched on when both numbers of proton particle-states (or hole-states) and neutron particle-states (or hole-states) have non-zero values.

(*iv*) Interactions between proton particle-states and neutron hole-states,

$$\sum_{ijkl}\sum_{\lambda} v_{\lambda}^{\rm ph}(N,Z)\Big[\big[\hat{a}_{i,\pi}^{\rm p\dagger}\times\hat{a}_{j,\nu}^{\rm h\dagger}\big]^{(\lambda)}\times\big[\hat{a}_{k,\pi}^{\rm p}\times\hat{a}_{l,\nu}^{\rm h}\big]^{(\lambda)}\Big]_{0}^{(0)},$$

or interactions between neutron particle-states and proton hole-states,

$$\sum_{ijkl}\sum_{\lambda} v_{\lambda}^{\rm ph}(N,Z)\Big[\big[\hat{a}_{i,\nu}^{\rm p\dagger}\times\hat{a}_{j,\pi}^{\rm h\dagger}\big]^{(\lambda)}\times\big[\hat{a}_{k,\nu}^{\rm p}\times\hat{a}_{l,\pi}^{\rm h}\big]^{(\lambda)}\Big]_{0}^{(0)},$$

which are switched on when both numbers of proton particle-states (or hole-states) and neutron hole-states (or particle-states) have non-zero values.

We note that proton particle-states and proton hole-states (or neutron particle-states and neutron hole-states) do not coexist by definition. We include necessary interactions into the Hamiltonian with proper two-body matrix elements evaluated in Sec. III A concerning the number of particles and holes in the $1f_{7/2}$ orbit [21].

2. *Illustrative example: Scandium isotopes*

Using the interpolation technique explained in Sec. III A, we have evaluated two-body matrix elements for nuclei in the $20 \leq N\,(Z) \leq 28$ region. We then calculate energy spectra of all those nuclei using the numerical code, `ArbModel`. Here, we just show results of scandium isotopes as an illustrative example, instead of showing all the results for 52 nuclei ($8\times 8 = 64$ nuclei except for 12 nuclei with 0p0h, 1p0h, and 0p1h configurations), since it would be good enough to demonstrate usefulness of our method.

Two-body matrix elements for scandium isotopes have been evaluated by a horizontal interpolation along the $Z = 21$ line by Eq. (8). In practical calculations, we apply particle-particle matrix elements $v_{\lambda}^{\rm pp}$ for ${}^{42-45}_{21}{\rm Sc}_{21-24}$ which have one-proton-particle and one- to four-neutron-particle states in terms of the Z and $N = 20$ cores. While we apply particle-hole matrix elements $v_{\lambda}^{\rm ph}$ for ${}^{46-48}_{21}{\rm Sc}_{25-27}$ which have one-proton-particle and one- to three-neutron-hole states in terms of the $Z = 20$ and $N = 28$ cores. Thus, this comparison would be a good validity check of the interpolation method with the (inverted) Pandya transformation. We note that, because of the particle-hole symmetry in the two-body matrix elements, resulting spectra of scandium isotopes ($Z = 21$) are equivalent to those of $N = 21$ isotones.

We concentrate only on states associated with couplings of particle(s) and/or hole(s) in the $1f_{7/2}$ orbit: $J^{\pi} = 0^{+}, 1^{+}, \cdots, 7^{+}$ states for even-A nuclei, $J^{\pi} = 1/2^{-}, 3/2^{-}, \cdots, 13/2^{-}$ states for odd-A nuclei. In Table V, we show low-lying energy spectra of ${}^{42-48}_{21}{\rm Sc}_{21-27}$ calculated by the `ArbModel` using the evaluated two-body matrix elements. We also show measured spectra reported in Ref. [13].

In the table, we put parentheses when the spin-parity of those states have not been identified yet. Because we could not find any candidates for $J^{\pi} = 13/2^{-}$ state of ${}^{45}_{21}{\rm Sc}_{24}$ and ${}^{47}_{21}{\rm Sc}_{26}$ in the experimental spectra, we put hyphens, "−", into the corresponding place in the table. We note that spectra of ${}^{42}_{21}{\rm Sc}_{21}$ and ${}^{48}_{21}{\rm Sc}_{27}$ completely coincide with the measurements by definition. We also note that, in the case of odd-even and odd-odd nuclei, there are a number states at low excitation energy. Correspondingly, we arbitrary select the most probable state for each J^{π} near the predicted value of the shell-model calculation. We indeed put asterisks, "∗", in the table, when there exist other states with the same J^{π} at lower excitation energy.

From the table, we find a fairly good agreement between the shell-model predictions and the measured spectra. Although there exists the ambiguity of the arbitrary selection of corresponding states from a number of states emerging at low excitation energy in odd-A nuclei, this good agreement may present usefulness of our method. We would be able to get many matrix elements by the interpolation technique for nuclei in a wide mass region which can be used to analyze abundant nuclei generated though the MNT reaction.

IV. SUMMARY AND PERSPECTIVE

In this report, we showed our motivation and the aim of this project and presented tentative results obtained so far to make it clear where we are on the way to accomplish the project.

The idea of this project is to obtain a deeper insight into microscopic mechanisms of multinucleon transfer (MNT) reactions by conducting several kinds of calculations for the structure of atomic nuclei. We consider three different approaches, the shell-model, the theory of coefficients of fractional parentage (c.f.p.), and the time-dependent Hartree-Fock (TDHF) theory com-

TABLE V. Low-lying excitation energies of scandium isotopes. Spectra obtained from the shell-model calculations using the `ArbModel` with two-body matrix elements evaluated by the interpolation technique are shown in comparison with experimental data. Experimental data have been taken from Ref. [13]. Energies with parenthesis mean that its spin-parity, J^π, has not been identified yet. States which have not been measured are represented by hyphens, "−". Energies with an asterisk " * " indicate the fact that an arbitrary selection from several candidate states for the spin-parity was done (see text).

	$^{42}_{21}$Sc$_{21}$		$^{43}_{21}$Sc$_{22}$		$^{44}_{21}$Sc$_{23}$		$^{45}_{21}$Sc$_{24}$		$^{46}_{21}$Sc$_{25}$		$^{47}_{21}$Sc$_{26}$		$^{48}_{21}$Sc$_{27}$	
J^π	Thr.	Exp.	Thr.	Exp.	Thr.	Exp.	Thr.	Exp.	Thr.	Exp.	Thr.	Exp.	Thr.	Exp.
7^+	0.616	(0.616)			1.039	0.968			0.963	0.978			1.096	1.096
$13/2^-$			3.390	(4.157)			2.454	–			2.241	–		
6^+	3.242	(3.242)			0.190	0.271			0.000	0.052			0.000	0.000
$11/2^-$			2.282	1.829			1.353	1.237			1.119	1.147		
5^+	1.510	(1.510)			1.151	1.531			0.276	0.281			0.131	0.131
$9/2^-$			1.630	(1.882)			1.502	1.662			1.668	1.878		
4^+	2.815	2.815			0.610	0.350			0.153	0.000			0.252	0.252
$7/2^-$			0.000	0.000			0.000	0.000			0.000	0.000		
3^+	1.490	1.490			0.675	0.762			0.208	0.228			0.623	0.623
$5/2^-$			3.344	3.463*			1.695	(2.093)*			1.452	1.297		
2^+	1.586	1.586			0.000	0.000			0.369	0.444			1.143	1.143
$3/2^-$			2.927	(2.984)*			1.639	(1.556)*			1.200	0.807		
1^+	0.611	0.611			0.345	0.667			1.421	0.991			2.517	2.517
$1/2^-$			4.256	(4.665)*			2.062	(2.151)			2.617	(2.810)		
0^+	0.000	0.000			2.993	2.779			4.953	(5.022)*			6.678	6.678

bined with the quantum-number projection technique (TDHF+QNP), which are based on different theoretical frameworks. While the shell-model and the theory of c.f.p. describe *static* excitation spectra, the TDHF+QNP method would describe structure of nuclei including effects of reaction *dynamics*. By comparing results obtained from those three different approaches, we consider that we may get a deeper understanding of microscopic reaction mechanisms.

Up to now, we have investigated how to evaluate two-body matrix elements for nuclei in a wide mass region which are necessary for the shell-model calculation. In this report, we have proposed a simple interpolation technique to evaluate the matrix elements for a bunch of nuclei from some available experimental data. As a first step, we consider nuclei having valence nucleons in the $1f_{7/2}$ orbit on top of the $N = 20$ and $Z = 20$ cores. We evaluated particle-particle (hole-hole) and particle-hole matrix elements for all nuclei in the $20 \leq N\,(Z) \leq 28$ region except for nuclei with 0p0h, 1p0h, and 0p1h configurations.

Using the evaluated matrix elements, we performed shell-model calculations by using the `ArbModel`. To check how our method works in practice, we compared calculated low-lying energy spectra of scandium isotopes with experimental spectra. From the comparison, we have found a fairly good agreement with the experimental data. We thus consider that our interpolation technique would be useful to calculate energy spectra of a number of nuclei which would be produced through the MNT reaction.

There are two remaining steps to accomplish this project. One is investigations of energy spectra using the theory of c.f.p. which gives us energy spectra generated by couplings of valence nucleons in a single-j orbit. The other is investigations of energy spectra for reaction products after MNT reactions. Recently, we have developed a theoretical framework to calculate expectation values of operators in a particle-number projected TDHF wave function after collision [9]. By extending the method to include parity and total angular momentum projections, it would be possible to calculate energy spectra specified by the spin-parity, J^π, directly from the TDHF wave function after collision. The implementation of the method into our numerical code is now in progress. By combining these three approaches, we may get a deeper insight into the reaction mechanisms which would enable us to answer interesting questions: "From which orbitals to which ones, nucleons are transferred?", "What kinds of states are populated after the MNT reaction?", "Can those populated states be described by the shell-model and/or c.f.p. predictions?", and so on.

ACKNOWLEDGMENTS

The author would especially thank Professor P. Van Isacker for giving valuable comments for proceeding the project. The author would be very much grateful for all the organizers and lecturers, secretaries and staffs in

GANIL, and managers of the dorm building, and other people who had been involved to held the wonderful and successful school. The author would like to thank all the participants of the school who had shared both joys and troubles during that fantastic period, *e.g.* successful evening sessions, exciting football games, a wonderful double-rainbow, and so on. This work was carried out as a project work of the TALENT initiative (TALENT: Training in Advanced Low Energy Nuclear Theory) course #5 "Theory for exploring nuclear structure experiments" held at GANIL, Caen, France, in August 11-29, 2014.

[1] L. Corradi, G. Pollarolo, and S. Szilner, J. Phys. G **36**, 113101 (2009).
[2] L. Corradi, J.H. He, D. Ackermann, A.M. Stefanini, A. Pisent, S. Beghini, G. Montagnoli, F. Scarlassara, G.F. Segato, G. Pollarolo, C.H. Dasso, and A. Winther, Phys. Rev. C **54**, 201 (1996).
[3] L. Corradi, A.M. Stefanini, J.H. He, S. Beghini, G. Montagnoli, F. Scarlassara, G.F. Segato, G. Pollarolo, and C.H. Dasso, Phys. Rev. C **56**, 938 (1997).
[4] L. Corradi, A.M. Vinodkumar, A.M. Stefanini, E. Fioretto, G. Prete, S. Beghini, G. Montagnoli, F. Scarlassara, G. Pollarolo, F. Cerutti, and A. Winther, Phys. Rev. C **66**, 024606 (2002).
[5] S. Szilner, L. Corradi, G. Pollarolo, S. Beghini, B.R. Behera, E. Fioretto, A. Gadea, F. Haas, A. Latina, G. Montagnoli, F. Scarlassara, A.M. Stefanini, M. Trotta, A.M. Vinodkumar, and Y. Wu, Phys. Rev. C **71**, 044610 (2005).
[6] S. Szilner, C.A. Ur, L. Corradi, N. Mărginean, G. Pollarolo, A.M. Stefanini, S. Beghini, B.R. Behera, E. Fioretto, A. Gadea, B. Guiot, A. Latina, P. Mason, G. Montagnoli, F. Scarlassara, M. Trotta, G. de Angelis, F. Della Vedova, E. Farnea, F. Haas, S. Lenzi, S. Lunardi, R. Mărginean, R. Menegazzo, D.R. Napoli, M. Nespolo, I.V. Pokrovsky, F. Recchia, M. Romoli, M.-D. Salsac, N. Soić, and J.J. Valiente-Dobón, Phys. Rev. C **76**, 024604 (2007).
[7] K. Sekizawa and K. Yabana, Phys. Rev. C **88**, 014614 (2013).
[8] K. Sekizawa and K. Yabana, to appear in EPJ Web of Conferences; arXiv:1403.2862 [nucl-th].
[9] K. Sekizawa and K. Yabana, Phys. Rev. C **90**, 064614 (2014).
[10] K. Sekizawa and K. Yabana, to appear in JPS Conference Proceedings; arXiv:1409.8612 [nucl-th].
[11] C. Simenel, Phys. Rev. Lett. **105**, 192701 (2010).
[12] P. Ring and P. Schuck, *"The Nuclear Many-Body Problem"* (Springer-Verlag, 1980).
[13] National Nuclear Data Center (NNDC), [`http://www.nndc.bnl.gov/chart/`].
[14] T.W. Burrows, Nuclear Data Sheets **107**, 1747 (2006).
[15] S. Zerguine and P. Van Isacker, Phys. Rev. C **83**, 064314 (2011).
[16] G. Audi, A.H. Wapstra, and C. Thibault, Nucl. Phys. **A729**, 337 (2003).
[17] D. Lunney, J.M. Pearson, and C. Thibault, Rev. Mod. Phys. **75**, 1021 (2003).
[18] S.P. Pandya, Phys. Rev. **103**, 956 (1956).
[19] I. Talmi, *Simple Models of Complex Nuclei. The Shell Model and Interacting Boson Model* (Harwood, Academic, Chur, 1993).
[20] S. Heinze, Ph. D. Thesis, der Universität zu Köln, Köln, Germany, 2008.
[21] When we construct input files of the `ArbModel`, we actually multiply $-\sqrt{2\lambda+1}/2$ for matrix elements between two like-particles (neutron-neutron or proton-proton) and $\sqrt{2\lambda+1}$ for matrix elements between two different kinds of particles (neutron-proton), since the `ArbModel` does not use isospin basis but uses neutron-proton basis.